HHS Public Access

Author manuscript

J Mech Behav Biomed Mater. Author manuscript; available in PMC 2022 April 01.

Published in final edited form as:

J Mech Behav Biomed Mater. 2021 April ; 116: 104342. doi:10.1016/j.jmbbm.2021.104342.

Biomechanical Properties of Acellular Scar ECM during the Acute to Chronic Stages of Myocardial Infarction

Bryn L. Brazile[2], **J. Ryan Butler**[2], **Sourav S. Patnaik**[2], **Andrew Claude**[2], **Raj Prabhu**[2], **Lakiesha N. Williams**[2,6], **Karla L. Perez**[1], **Kytai T. Nguyen**[1], **Ge Zhang**[5], **Pietro Bajona**[4], **Matthias Peltz**[4], **Yong Yang**[3], **Yi Hong**[1], **Jun Liao**[1,*]

[1]Department of Bioengineering, University of Texas at Arlington, Arlington, TX 76019

[2]Department of Biological Engineering and College of Veterinary Medicine, Mississippi State University, MS, 39762

[3]Department of Biomedical Engineering, University of Northern Texas, Denton, TX 76203

[4]Department of Cardiovascular and Thoracic Surgery, University of Texas Southwestern Medical Center, Dallas, TX 75390.

[5]Department of Biomedical Engineering, University of Akron, Akron, OH, 44325

[6]Department of Biomedical Engineering, University of Florida, Gainesville, FL 32611

Abstract

After myocardial infarction (MI), the infarcted tissue undergoes dynamic and time-dependent changes. Previous knowledge on MI biomechanical alterations has been obtained by studying the explanted scar tissues. In this study, we decellularized MI scar tissue and characterized the biomechanics of the obtained pure scar ECM. By thoroughly removing the cellular content in the MI scar tissue, we were able to avoid its confounding effects. Rat MI hearts were obtained from a reliable and reproducible model based on permanent left coronary artery ligation (PLCAL). MI heart explants at various time points (15 minutes, 1 week, 2 weeks, 4 weeks, and 12 weeks) were subjected to decellularization with 0.1% sodium dodecyl sulfate solution for ~1–2 weeks to obtain acellular scar ECM. A biaxial mechanical testing system was used to characterize the acellular scar ECM under physiologically relevant loading conditions. After decellularization, large decrease in wall thickness was observed in the native heart ECM and 15 minutes scar ECM, implying the collapse of cardiomyocyte lacunae after removal of heart muscle fibers. For scar ECM 1 week, 2 weeks, and 4 weeks post infarction, the decrease in wall thickness after decellularization was small. For scar ECM 12 weeks post infarction, the reduction amount of wall thickness due to decellularization was minimal. We found that the scar ECM preserved the overall

*Corresponding author: Jun Liao, PhD, Tissue Biomechanics & Bioengineering Laboratory, Department of Bioengineering, University of Texas at Arlington, 500 UTA BLVD, Suite 353, Arlington, TX 76010, Tel: (817) 272-6779, jun.liao@uta.edu.

Author Statement

All authors declare that there is no proprietary, financial, professional or other personal interest of any nature or kind that could inappropriately influence (bias) the work presented in this manuscript.

mechanical anisotropy of the native ventricle wall and MI scar tissue, in which the longitudinal direction is more extensible. Acellular scar ECM from 15 minutes to 12 weeks post infarction showed an overall stiffening trend in biaxial behavior, in which longitudinal direction was mostly affected and manifested with a decreased extensibility and increased modulus. This reduction trend of longitudinal extensibility also led to a decreased anisotropy index in the scar ECM from the acute to chronic stages of MI. The post-MI change in biomechanical properties of the scar ECM reflected the alterations of collagen fiber network, confirmed by the histology of scar ECMs. In short, the reported structure-property relationship reveals how scar ECM biophysical properties evolve from the acute to chronic stages of MI. The obtained information will help establish a knowledge basis about the dynamics of scar ECM to better understand post-MI cardiac remodeling.

Keywords

Myocardial Infarction; Scar tissue; Extracellular matrix; Biaxial mechanical testing; agen fibers; Rat hearts

1. Introduction

Myocardial infarction (MI) affects more than 8 million Americans. Each year in the United States, the newly diagnosed cases of MI is estimated to be 620,000 and ~295,000 suffer from a recurrent MI, which means that approximately every 34 seconds an American has an MI (1). MI causes massive heart cell death and degradation of heart extracellular matrix (ECM), followed by the formation of scar tissue mediated by cardiac fibrosis (2–5). The post-MI remodeling alters the biomechanics and contractile function of the ventricular walls and contiguously debilitates cardiac function, eventually resulting in heart failure (3–5).

In a healthy heart, the interaction between the myocardial ECM and heart muscle fibers is well coordinated and balanced (6–13). The myocardial ECM network has a honeycomb morphology, with well-organized pores for the residing of heart muscle fibers (cardiomyocyte lacuna) (6–9). This intriguing myocardial ECM network consists of dominantly collagen fibers (type I and III), along with proteoglycans and sparsely distributed elastin fibers (6–9). The ECM fibers bind the heart muscle fibers together, transfer loads among muscle fibers and hence mediate their contraction/relaxation, and prevent excessive stretching (10–12). In an event of an MI, both the cardiomyocytes and myocardial ECM experience drastic alterations. The infarct tissue after acute ischemia experiences a dynamic and time-dependent process, which consists of three phases: (i) necrotic phase, (ii) fibrotic phase, and (iii) remodeling phase – each exhibiting unique structural and mechanical properties (13–17).

Necrosis of cardiomyocytes occurs within 30 minutes post-MI, and the site of infarction develops necrotic tissue – a change that is irreversible if there is no immediate clinical intervention (15–17). The necrotic phase of MI begins a few hours after acute ischemia and ends after approximately 7 days in human (18). Within hours after acute ischemia, infarcted myocardium loses its characteristic striations and the left ventricle became more compliant (19). Increased matrix metalloproteinase (MMP) activity, a drop in collagen content, and a

breakdown of ECM glycoproteins have been reported during the period of increasing left ventricle compliance (20, 21). At the end of necrosis the formation of new ECM components begins and a scaffold for new collagen deposition is prepared; at the tissue level, the ventricular compliance stops increasing, and tissue stiffening starts (11, 15, 16, 25).

In the following fibrotic phase, myofibroblasts can increase 20-fold (22, 23), and these highly active myofibroblasts deposit a large amount of collagen (18, 19, 24). This results in an increase in stiffness and a distinctive anisotropy in the infarcted tissue, with both circumferential and longitudinal stiffness appear to increase under multiaxial loading (11, 15, 16, 25). In a pig model, 3 weeks after an MI was produced, the scar was found to be predominantly type I collagen fibers, which were highly aligned in each transmural layer with a pattern similar to that of native myocardium (26).

The remodeling phase begins at 3–4 weeks, and the stiffness begins to decrease and this effect appears unrelated to collagen content (11, 18, 24). The remodeling phase does not have a clear cut endpoint due to the dynamic and continually changing nature of the tissue. In the remodeling phase, the increase in collagen content slows down but crosslinking increases, and the infarct is observed to shrink topographically (11, 13, 14, 25, 27–35). Overall, the global modulus of the scar tissue was found to depend on the amount of fibrotic collagen, the degree of crosslinking, as well as fiber distribution (11, 13, 14, 25, 28–35).

The above-mentioned knowledge on MI biomechanical alterations has been obtained by studying the explanted scar tissue, and there has not been a study on the biomechanical evolution at pure scar ECM level. The scar ECM not only plays a pivotal role in the development and progression of MI (25, 29, 32, 34, 35), but is also thought to be a barrier for effective and efficient therapy of exogenous stem cells (36–44). Recently, several *in vitro* studies have shown that ECM/scaffold stiffness plays a crucial role in the regulation of stem cell cardiac differentiation (44–54), indicating the need to better understand ECM/scaffold micromechanics.

From cellular perspective, in the necrotic phase neutrophils, macrophages, and lymphocytes infiltrate the infarct for removal of dead cardiomyocytes and necrotic debris (55, 56). When reaching the fibrotic phase, the MI scar tissue consists of highly proliferated, active myofibroblasts and the deposited fibrotic collagen fiber network, along with adhesive proteins such as fibronectin, laminins, matricellular proteins, and metalloproteinases (57–60). The proportion of the fibrotic collagen and myofibroblasts (major cellular content) changed along with the post-MI stages and time (57–60). The use of the decellularized scar ECM enabled us to more accurately assess the structural and biomechanical evolution of cardiac microenvironment post-MI. By thoroughly removing the cellular content in the MI scar tissue, we were able to avoid its confounding effects.

We hence initiated the study of the pure scar ECM by applying a decellularization technique to MI scar tissues created by permanent left coronary artery ligation (PLCAL) in a rat model. Decellularization is a tissue treatment technique that uses chemical, enzymatic, or physical treatment methods lasting from a few hours to days to remove the cellular content and chromosome material from the tissue, with a goal to obtain acellular ECM scaffolds

(61–66). These methods work by disrupting the cell membrane which releases the cellular contents that are then rinsed away (62, 66). In return, the acellular ECM scaffolds of a specific tissue can be obtained, with the overall structural and mechanical intergrity preserved (67–69).

By quantifying the biophysical properties of pure scar ECM, we can build a thorough dataset that delineates the time course changes in scar ECM anisotropy, extensibility, stiffness, as well as structural parameters such as collagen fiber alignment. The obtained information not only helps establish a knowledge basis about the dynamics of scar ECM at various post-MI stages, but also sheds light on the local biomechanical environment of the scar tissue, which will be an important consideration when designing optimal cell therapy. Our new method thus adds new perspective to the knowledge obtained via traditional approaches based only on MI tissue samples (11, 14, 25, 28–35, 70).

2. Materials and Methods

2.1 Create MI rat hearts using PLCAL

The rat animal protocol was approved by the Mississippi State University Institutional Animal Care and Use Committee (IACUC, #12–024) and was performed in accordance with the National Institutes of Health (NIH, Bethesda, MD, USA) guidelines. Surgical procedures were adopted from the previous publications (71, 72). Thirty-six Sprague-Dawley rats (~300–350 g) were used during a 12-week period (n=6 for each time point). Briefly, the rats were placed under anesthesia with a mixture of oxygen and 5.0% isoflurane, then intubated with a 16-gauge intravenous catheter. The rat's body temperature (96.6–99.5°F) was maintained during the procedure by a heated operating pad. Positive-pressure ventilation was established, and anesthesia was maintained with a mix of oxygen/2.0% isoflurane throughout the surgery. A left thoracotomy was performed at the 4th intercostal space and ribs were retracted followed by a pericardiotomy. For the control group, the rats were euthanized by arresting the heart in diastole via intra-cardiac injection of saturated potassium chloride solution. The hearts were then harvested and stored in phosphate buffered saline (PBS) at 4 °C.

For rats in the MI groups, an MI was generated by a reliable and reproducible model based on PLCAL. The PLCAL was induced 2–3 mm distal to the auricular appendix with a 6–0 non-absorbable Polypropylene suture. For rats in the 15-minute post-MI group, the animals were euthanized following the same procedure as the control group after waiting 15 minutes following successful ligation of the artery. For all other MI groups (1, 2, 4, and 12 weeks post-MI), the chest cavity was immediately closed, and the animal was given subcutaneous buprenorphine injection for postoperative pain management. At the pre-determined harvest time point (1, 2, 4, and 12 weeks post-MI), each rat was placed back under anesthesia, the chest cavity reopened, and the rats were euthanized with the same procedure as before (Figure 1). In short, the infarcted hearts were harvested at 15 minutes post MI (15M), 1 week post MI (1W), 2 weeks post MI (2W), 4 weeks post MI (4W), and 12 weeks post MI (12W), to capture post-MI responses from the acute to chronic stages, i.e., necrotic phase, fibrotic phase, and remodeling phase (11, 13, 14, 25, 28–35). During the first minutes to hours after a myocardial infarction, inflammation and necrosis are the major pathological

processes, and the necrotic phase lasts to about 1 week (18). The fibrotic phase oversees the deposition of fibrotic collagen and increased tissue stiffness and lasts about 3 – 4 weeks (11, 18, 24). The MI tissue then enter remodeling phase, in which the scar tissue experiences a gradual adjustment and maturation, such as a decreased collagen deposition rate and an increase of collagen crosslinking. The remolding phase shows that the MI reaches chronicle stage and can last for months (11, 18, 24, 26, 70).

2. 2 Obtaining the Pure Scar ECM via Decellularization

The scar tissue formation was observed below the ligation site in the left ventricle portion of the infarcted hearts. The PLCAL successfully produced scar tissue at a variety of degrees at different time points on the heart explants. The left and right atriums, pulmonary artery, and aortic artery were carefully removed from the heart explants. After measuring the wall thickness of the scar region with a digital caliper, the ventricles were subjected to an optimized decellularization protocol to obtain pure scar ECM (73–75). The ventricles were decellularized in a rotating bioreactor using decellularization solution made of 0.1% sodium dodecyl sulfate (SDS) (Sigma Aldrich Inc., St. Louis, MO), 0.01% trypsin (VWR), 1 mM phenylmethylsulfonylfluoride (PMSF, protein inhibitor) (Sigma Aldrich), 20 μg/ml RNase A (Sigma Aldrich), 0.2 mg/ml DNase (Sigma Aldrich), and 100 U/ml penicillin and 100 μg/ml streptomycin (Sigma Aldrich). The decellularization was performed at room temperature for ~1–2 weeks to achieve a full decellularization. Ten-minute ultrasonic treatment (50 Hz) was applied each day, and the decellularization solution was changed every day to avoid contamination and tissue deterioration. After the complete removal of cellular contents, the acellular heart tissues showed an appearance of pale white color, similar to our previously reported studies (54, 73–75).

2.3 Ventricular Wall Thickness Measurements

Thickness measurements were taken on the LV scar region before and after decellularization. For both the scar tissue and the acellular scar ECM, the thickness of each sample was taken in triplicate and averaged for each time point using a digital caliper (Mityoso, Inc). Following the thickness measurement, the acellular scar ECM was trimmed as a square specimen for biaxial mechanical testing and then histological characterization.

2.4 Biaxial Mechanical Testing of the Acellular Scar ECM

A custom-built biaxial mechanical testing system was used to characterize the anisotropic mechanical behavior of planar soft tissues under physiologically-relevant loading conditions (73, 76–78). Square specimens (~ 10 mm × 10 mm × 1 mm) were trimmed from the LV scar region, with one axis aligned with the longitudinal direction and the other with the circumferential direction. Each side of the square specimen was mounted onto four stainless steel hooks that were attached to two loops of 000 polyester sutures. Four fiducial graphite markers, affixed to the center of the square specimen with cyanoacrylate adhesive, were monitored via a CCD camera to record the real time tissue deformation. The specimen was preconditioned for 10 cycles by applying biaxial tension up to 30 N/m along both the longitudinal direction (T_L = 30 N/m) and circumferential direction (T_C = 30 N/m) (73). Lagrangian membrane tension was calculated by normalizing the force to the initial length of the specimen edge. Tension higher than 30 N/m was found to cause tissue tear at the

hook, and we thus set 30 N/m as the maximum tension in our biaxial testing. After preconditioning, the final equibiaxial tension protocol of T_L:T_C = 30:30 N/m was performed to capture the biaxial behavior.

From the biaxial mechanical curves, we derived the following parameters: areal strain at 30:30 N/m, anisotropy index, extensibilities at 30:30 N/m, and modulus at certain strain level. Extensibilities were defined as the maximum stretch ratios at 30:30 N/m, as λ_L for longitudinal direction and λ_C for circumferential direction. Areal strain at 30:30 N/m could be then calculated as follows:

$$Areal\ Strain = (\lambda_L * \lambda_C - 1) * 100\% \quad (1)$$

where λ_L and λ_C are, as we just defined, the maximum stretch ratios at 30:30 N/m for longitudinal and circumferential directions, respectively.

Moreover, anisotropy index can be calculated as equation (2), representing the directional variation of tissue mechanical behavior:

$$Anisotropy = (\lambda_L - \lambda_C)/\frac{(\lambda_L + \lambda_C)}{2} \quad (2)$$

In this study, we further examined the tangent modulus of the longitudinal direction at the stretch level of 1.03, which corresponded to the transitional region of the curve.

2.5 Histology and Collagen Fiber Alignment

To reveal the collagen fiber microstructure, the acellular scar ECM samples and an acellular native ECM sample were submerged in 2% paraformaldehyde for fixation for 72 hours before histological preparation. Histological sectioning at 5 μm thick was performed via an in-plane cutting technique. Histological slides were then stained with Picrosirius Red (collagen fibers appear red). Images were taken using a Leica Microsystems DB2500 microscope at 10× magnification under bright field. To quantify the overall collagen fiber alignment, the bright field images were converted to 8-bit images for ImageJ analysis. Using the OrientationJ plugin in ImageJ, we were able to determine collagen fiber distribution from −90 degrees to 90 degrees (79). Area under the curve (AUC) was then determined for each of the collagen fiber distributions. Picrosirius Red stained slides were further imaged using polarized light microscopy to identify Type I (yellow-red) and III collagen (green) with appropriate band-pass filters (80, 81).

2.6 Statistical Analysis

Data were reported as mean ± standard deviation. One-way analysis of variances (ANOVA) was used to determine if the parameters were statistically different among the groups, with Tukey's test for post hoc pair-wise comparison. A paired t-test was utilized to determine if the thickness measurements before and after decellularization were significantly different. Data was considered significant when $p < 0.05$. Statistical analysis was performed using SPSS software (version 23; SPSS Inc., Chicago, IL).

3. Results

3.1 Gross Anatomical Observation

After decellularization, the photographic images of acellular control hearts and the acellular MI hearts were taken and presented side by side with the rat hearts before decellularization (Figure 2). We found that the PLCAL procedures successfully created MIs in the mid and apical regions of the rat left ventricle, and the MI-induced scar tissue with pale whitish color was clearly observed in all the heart explants harvested at time points of 1 week, 2 weeks, 4 weeks, and 12 weeks post-MI (Arrows in Figure 2-E, G, I, K). For the heart explants harvested 15 minutes post-MI, the region below the ligation site showed a slightly pale color (Figure 2-C) compared with the surrounding tissue, implicating ischemic response due to PLCAL.

When comparing the acellular hearts with the native hearts, we found that the native hearts showed a degree of dark red colors, a color tone from native heart muscle morphology, and overall the acellular hearts appeared pale white, indicating the removal of cellular contents of the heart via the decellularization procedure. More specifically, we noticed that (i) the acellular scar ECM samples from the control and 15M were clear and translucent (Figure 2-B, D); (ii) the acellular scar ECM samples from 1W, 2W, and 4W hearts exhibited a more solid whitish color (Figure 2-F, H, J); whereas (iii) the acellular scar ECM from 12W showed a gray color (Figure 2-L). We found that the longer the post-MI interval, the more decellularization time was needed to achieve complete decellularization. This phenomenon was likely due to the difference in content of both scar ECM and heart ECM at the different stages of an MI.

3.2 Change in Wall Thickness

The wall thickness of the scar tissues, i.e., wall thickness measured before the decellularization, showed an overall decrease as the post-MI time increased (One-way ANOVA, $p < 0.005$). Post hoc comparison results using the Tukey's test indicated that the average thickness for the 12W scar tissue (1.94±0.10 mm) was significantly different from the following groups: native tissue (2.56±0.26 mm), 15M (2.67±0.10 mm), 1W (2.63±0.13 mm), 2W (2.48±0.24 mm), and 4W post-MI tissues (2.55±0.22 mm) as summarized in Figure 3.

For the thickness of the acellular scar ECMs, we found that there was a statistically significant difference among the different time points (One-way ANOVA, $p < 0.005$). Post hoc comparison results using the Tukey's test indicated that the average thickness for the native ECM (0.64±0.23 mm) was significantly different from the following groups: 1W (1.95±0.19 mm), 2W (1.96±0.18 mm), 4W scar ECM (1.90±0.27 mm), and 12W scar ECMs (1.85±0.10 mm) (Figure 3). Additionally, the average thickness for the 15M post-MI ECM (1.26±0.30 mm) was also significantly different compared to the 1W, 2W, and 12W scar ECM groups (Figure 3).

When comparing the wall thickness before and after decellularization treatment (including the native control and MI groups), we found an overall reduction in thickness (Figure 3). Reduction in thickness was at a maximum of ~75% decrease for the decellularized native

tissue (control group). The percent reduction in thickness decreased when post-MI time increased (15M to 12W). The least change was in the 12W group (~5% reduction). The percentage of thickness reductions in the 1W (~26%), 2W (~21%), and 4W group (~25%) were found to be similar in magnitude. The percentage of wall thickness reduction was assessed with paired t-test at each time point and suggested that the thickness reduction at each time point was significant ($p < 0.05$).

3.3 Biaxial Mechanical Behavior of Scar ECM

The stress vs stretch plots from the decellularized scar tissues are shown in Figure 4. The biaxial mechanical curves showed that the acellular native heart ECM and acellular scar ECM had in fact preserved the overall anisotropy that has been observed in rat ventricle tissue and rat scar tissue (25, 29, 32, 34, 35), i.e., the longitudinal direction being more extensible than the circumferential direction. We found that with the increase of post-MI time, the longitudinal direction of the acellular scar ECM experienced a stiffening trend (Figure 4B–F), whereas the circumferential direction of the acellular scar ECM did not show an obvious trend. Nevertheless, the circumferential direction of the acellular scar ECM (Figure 4B–F) was overall more extensible than the circumferential direction of the native ECM (Figure 4A). The overall stiffening trend post-MI was further evidenced by analyzing the areal strains of the native ECM and the acellular scar ECMs at various post-MI time points ($p=0.0015$, Figure 5A). Post hoc pairwise comparison results using the Tukey's test indicated that the areal strain for the 15M group (10.38±1.27%) was significantly different from the following groups: 4W group (7.11±0.85%), and 12W group (7.74±0.74%). Anisotropy index was found to significantly decrease from the native ECM group to 12W group ($p=0.006$), with the 12W group showing the least anisotropy (Figure 5B). Post hoc pairwise comparison indicated that the anisotropy index for the 12W group (0.011±0.004) was significantly different from the following groups: native ECM group (0.052±0.021), and 15M group (0.041±0.004).

Extensibility along the longitudinal direction had an overall significant decreasing trend from the native ECM group to the 12W group ($p=0.002$) (Figure 5C). Post hoc comparison results using the Tukey's test indicated that the longitudinal extensibility for the native group (1.075±0.022) was significantly different from the following groups: 4W group (1.048±0.009), and 12W group (1.044±0.003). Additionally, the Tukey's test indicated that 15M group (1.072±0.013) was significantly different from the 12W group (1.044±0.003). Longitudinal direction modulus, estimated at the transitional region of the nonlinear curve (1.02 – 1.04 stretch), was found to increase from the 15M group to the 12W group, while the 15 M group showed an evident softening when compared with the native group (Figure 5D). Post hoc comparison results using the Tukey's test indicated that the longitudinal modulus for the 15M group (192.332±78.360 kPa) was significantly different from the 12W group (440.268±86.520 kPa).

3.4 Microstructure of Scar ECM

For the native and 15 M groups, based on the large differences between the wall thickness before and after decellularization (Figure 3 – Native; 15 min), we concluded a large collapse of the cardiomyocyte lacunae (honeycomb lacunae structure) took place in the decellularized

native group and decellularized 15M group, and the large collapse was caused by complete removal of the cells that occupied a great volume space. The in-plane picrosirius red (Figure 6) stained images at 10× magnification confirmed our speculation of lacunae collapse when analyzing the wall thickness change after decellularization. The scar ECM of 1W, 2W, 4W, and 12W groups were found to exhibit increased scar collagen deposition (Figure 6). Polarized light microscopy images revealed an increase in collagen type I (yellow-red color) in 2W and 4W groups (Figure 7D,E), while 12W groups showed both dense collagen type I (yellow-red color) and type III (green color) (Figure 7F).

In-plane scar collagen fiber distribution was quantified from histological images (Figure 6). One limitation of the histological assessment in this study was caused by the loss of tissue orientation tracking (circumferential versus longitudinal) when the in-plane histological sectioning performed. The collagen fiber distributions had to be presented in a way that the fiber preferred direction was set as zero degree and the overall distribution was from −90 degree to +90 degree (Figure 8). Note that the zero degree in Figure 8 represents only the collagen fiber preferred direction and was not related to any anatomic orientation due to the above-mentioned limitation. The fiber distribution curves showed that collagen fibers in 1W and 2W scar ECM exhibited a much higher fiber alignment (Figure 8C,D). This trend, however, was not monotonic and the fiber alignment in the 4W and 12W groups (Figure 8E,F) decreased when compared with the 1W and 2W groups (Figure 8C,D).

4. Discussion

A reliable and reproducible rat PLCAL model was adopted to obtain infarcted hearts at varying post-MI time points (15M, 1W, 2W, 4W, and 12W post-MI). By ligating the left coronary artery, we produced MI hearts with an 80% survival rate for the rats undergoing surgery. By further applying an efficient decellularization protocol to the MI heart tissues, we obtained pure scar ECM from the acute to chronic stages of MI. After decellularization, there was a noticeable thinning of the left ventricle wall in the control group and 15M post-MI group (~75% and ~53%, respectively). We speculate that this profound ventricular wall thinning is likely due to the removal of the healthy cardiomyocytes from the control group and the removal of the ischemic cardiomyocytes from the 15M post-MI group, which leads to the collapse of the honeycomb-shaped pores fabricated with collagen fibers (i.e., cardiomyocyte lacunae)(74).

As the MI scar matured, myofibroblasts gathered in the infarcted area and started depositing excess collagen (82). This phase was captured by our thickness measurements before and after decellularization, i.e., the scar ECM obtained from the later stages of MI (1W, 2W, and 4W groups) had a smaller thickness reduction (~26%, ~21%, and ~25% respectively) compared with the control group (~75%) and 15M post-MI group (~53%), implicating the scar collagen network was much denser, while certain structural spacing (e.g., cellular content) still existed and collapsed after the decellularization treatment. However, by the 12W time point, the infarcted area entered a phase with a stable collagen structure and few residual myofibroblasts (83). Hence, the marginal thickness reduction in the 12W group (~5%) was likely due to the formation of mature scar, which increased collagen content and collagen crosslinking.

To our knowledge, this is the first report of the time-dependent biomechanical properties of the acellular scar ECM. We found that the acellular scar ECM preserved an overall anisotropy of the native ventricle wall and MI scar tissue, showing a more extensible longitudinal direction (72). Our observation of an overall stiffening trend in acellular scar ECM biaxial behavior from the acute to chronic stages of MI (Figure 4) was consistent with the previously reported stiffening trend of biaxial behavior in rat MI scar tissues (72). We noticed that the reduction in scar ECM extensibility was mainly occurring in the longitudinal direction (Figure 4, 5), indicating that the longitudinal direction experienced more behavior change due to structural alterations in MI progression. This reduction trend of longitudinal extensibility led to a decreased anisotropy index in the scar ECM biaxial behavior from the acute to chronic stages of MI. The anisotropy index was smallest at the 12W scar ECM group, which was due to the reduction of longitudinal extensibility as well as the increase of extensibility along the circumferential direction (Figure 4F). A less anisotropic mechanical behavior in the 12W scar ECM might be caused by a mature scar collagen network with more stable crosslinking. In Sirry's study, the rat MI scar tissue was also found to be stiffer in the circumferential direction than in longitudinal direction, and the mechanical anisotropy was observed up to 28 days (4 weeks) post-MI. Sirry et al interpreted that the mechanical anisotropy of MI scar tissues were related to collagen fiber orientation in the infarcts (72).

Previous histological studies of the infarcted hearts have shown that the collagen fibers in scar tissue tend to remain anisotropic, with the majority of the fibers aligned with the circumferential direction of the heart (25, 29, 32, 34, 35). One study on MI scar tissue revealed that the healing rat infarcts were isotropic both mechanically and structurally, with collagen fiber distribution showing the greatest deviation from random at 6 week (70). Existence of various observations could be attributed to the complex nature of MI studies, in which observations might be affected by the different animal species used in study, the size and location of the induced infarct, and the location-dependent nature of the scar collagen fiber orientation in MI hearts (72, 84–86). Future studies are thus warranted to collect more data on MI biomechanics and ultrastructure, and with additional data the above mentioned observations can be better understood.

The changes in biomechanical properties of the scar ECM post-MI implied a micro-environmental change, i.e., the increase of collagen content and the degree of collagen crosslinking. Our histological observations confirmed the ultrastructural alterations. From the histological images, the scar ECM ultrastructure showed a denser morphology along the time course of MI, consistent with the previous studies, which showed type I collagen content gradually increased after an MI (11, 13, 25, 70). The collapse of cardiomyocyte lacunae after decellularization was confirmed in the in-plane histology of the control group and the 15M group (Figures 6, and 7). Given that the histological images were used to calculate the fiber distribution, the lacunae collapse in the control group and 15M group could possibly skew the fiber distribution results for those two groups. Nevertheless, we were able to capture a good representation of the collagen fiber orientation from middle to late stages of MI with the lesser degree of ultrastructural collapse.

5. Conclusions

The major conclusions are as follows: (i) We successfully obtained pure scar ECM from the acute to chronic stages of MI by applying an efficient decellularization protocol to the rat MI scar tissue generated via a PLCAL model. (ii) The excess collagen deposition along the MI scar maturation was evidenced by the thickness measurements before and after decellularization, where the scar ECM obtained from the later stages of MI (1W, 2W, 4W, and 12 W groups) had a smaller thickness reduction (~26%, ~21%, ~25%, and 5%, respectively) compared with the control group (~75%) and 15M post-MI group (~53%). (iii) The acellular scar ECM preserved the overall mechanical anisotropy of the native ventricle wall and MI scar tissue, in which the longitudinal direction was more extensible. (iii) From the 15 minutes to 12 weeks post-MI, the acellular scar ECM showed an overall stiffening trend and a decreased anisotropy index in biaxial behavior, with the stiffening mostly caused by change in the longitudinal direction. (iv) The post-MI change in biomechanical properties of the scar ECM reflected the alterations of collagen fiber network, confirmed by the histology of scar ECMs. The obtained structure-property relationship revealed how scar ECM biophysical properties evolved from the acute to chronic stages of MI. This new approach improves traditional methods based only on MI scar tissue samples, where cell interference or presence may compromise accurate characterization and isolation of ECM characteristics. The obtained information will help establish a knowledge basis about the dynamics of scar ECM, which will improve our understanding of post-MI cardiac remodeling.

Acknowledgement

We thank the support of 13GRNT17150041 from AHA, 1R01EB022018–01 and T32 HL134613 from NIH, and UT STARS.

References

1. Go AS, Mozaffarian D, Roger VL, Benjamin EJ, Berry JD, Blaha MJ, et al. Heart disease and stroke statistics−−2014 update: a report from the American Heart Association. Circulation. 2014;129(3):e28.
2. Mozaffarian D, Benjamin EJ, Go AS, Arnett DK, Blaha MJ, Cushman M, et al. Heart Disease and Stroke Statistics—2016 Update A Report From the American Heart Association. Circulation. 2015:CIR. 0000000000000350.
3. Janicki JS, Brower GL, Gardner JD, Chancey AL, Stewart JA Jr., The dynamic interaction between matrix metalloproteinase activity and adverse myocardial remodeling. Heart failure reviews. 2004;9(1):33–42. [PubMed: 14739766]
4. Spinale FG, Janicki JS, Zile MR. Membrane-associated matrix proteolysis and heart failure. Circulation research. 2013;112(1):195–208. [PubMed: 23287455]
5. Tsuruda T, Costello-Boerrigter LC, Burnett JC Jr., Matrix metalloproteinases: pathways of induction by bioactive molecules. Heart failure reviews. 2004;9(1):53–61. [PubMed: 14739768]
6. Streeter D, Powers WE, Ross A, Torrent-Guasp F. Three-Dimensional Fiber Orientation in the Mammalian Left Ventricular Wall. Cardiovascular System Dynamics: M.I.T Press; 1978. p. 73.
7. Streeter DD Jr., Hanna WT Engineering mechanics for successive states in canine left ventricular myocardium. II. Fiber angle and sarcomere length. Circulation research. 1973;33(6):656–64. [PubMed: 4762007]

8. Streeter DD Jr., Spotnitz HM, Patel DP, Ross J Jr., , Sonnenblick EH Fiber orientation in the canine left ventricle during diastole and systole. Circulation research. 1969;24(3):339–47. [PubMed: 5766515]
9. Macchiarelli G, Ohtani O. Endomysium in left ventricle. Heart (British Cardiac Society). 2001;86(4):416. [PubMed: 11559682]
10. Weber KT. Cardiac interstitium in health and disease: the fibrillar collagen network. Journal of the American College of Cardiology. 1989;13(7):1637–52. [PubMed: 2656824]
11. Holmes JW, Borg TK, Covell JW. Structure and mechanics of healing myocardial infarcts. Annu Rev Biomed Eng. 2005;7:223–53. [PubMed: 16004571]
12. Humphery JD. Cardiovascular Solid Mechanics: Springer Verlag; 2002.
13. Fomovsky GM, Thomopoulos S, Holmes JW. Contribution of extracellular matrix to the mechanical properties of the heart. Journal of molecular and cellular cardiology. 2010;48(3):490–6. [PubMed: 19686759]
14. Herrmann KL, McCulloch AD, Omens JH. Glycated collagen cross-linking alters cardiac mechanics in volume-overload hypertrophy. American Journal of Physiology-Heart and Circulatory Physiology. 2003;284(4):H1277-H84.
15. Pirzada FA, Ekong EA, Vokonas PS, Apstein CS, Hood W. Experimental myocardial infarction. XIII. Sequential changes in left ventricular pressure-length relationships in the acute phase. Circulation. 1976;53(6):970–5. [PubMed: 1269134]
16. Vokonas PS, Pirzada FA, Hood WB. Experimental myocardial infarction: XII. Dynamic changes in segmental mechanical behavior of infarcted and non-infarcted myocardium. The American journal of cardiology. 1976;37(6):853–9. [PubMed: 1266750]
17. Pilia M Left ventricular mechanical properties post-myocardial infarction and the role of matrix metalloproteinase-9: ProQuest; 2008.
18. Fishbein MC, Maclean D, Maroko PR. The histopathologic evolution of myocardial infarction. Chest. 1978;73(6):843–9. [PubMed: 657859]
19. Forrester JS, Diamond G, Parmley WW, Swan HJ. Early increase in left ventricular compliance after myocardial infarction. The Journal of clinical investigation. 1972;51(3):598–603. [PubMed: 5011102]
20. Sato S, Ashraf M, Millard RW, Fujiwara H, Schwartz A. Connective tissue changes in early ischemia of porcine myocardium: an ultrastructural study. Journal of molecular and cellular cardiology. 1983;15(4):261–75. [PubMed: 6876183]
21. Etoh T, Joffs C, Deschamps AM, Davis J, Dowdy K, Hendrick J, et al. Myocardial and interstitial matrix metalloproteinase activity after acute myocardial infarction in pigs. American journal of physiology. 2001;281(3):H987–94. [PubMed: 11514263]
22. Fishbein MC, Maclean D, Maroko PR. Experimental myocardial infarction in the rat: qualitative and quantitative changes during pathologic evolution. Am J Pathol. 1978;90(1):57–70. [PubMed: 619696]
23. Yang F, Liu YH, Yang XP, Xu J, Kapke A, Carretero OA. Myocardial infarction and cardiac remodelling in mice. Exp Physiol. 2002;87(5):547–55. [PubMed: 12481929]
24. Richardson WJ, Clarke SA, Quinn TA, Holmes JW. Physiological Implications of Myocardial Scar Structure. Compr Physiol. 2015;5(4):1877–909. [PubMed: 26426470]
25. Holmes JW, Nunez JA, Covell JW. Functional implications of myocardial scar structure. American Journal of Physiology-Heart and Circulatory Physiology. 1997;41(5):H2123.
26. Holmes JW, Yamashita H, Waldman LK, Covell JW. Scar remodeling and transmural deformation after infarction in the pig. Circulation. 1994;90(1):411–20. [PubMed: 8026026]
27. Jugdutt BI, Amy RW. Healing after myocardial infarction in the dog: changes in infarct hydroxyproline and topography. Journal of the American College of Cardiology. 1986;7(1):91–102. [PubMed: 3941223]
28. Campbell PH, Hunt DL, Jones Y, Harwood F, Amiel D, Omens JH, et al. Effects of biglycan deficiency on myocardial infarct structure and mechanics. Molecular & cellular biomechanics: MCB. 2008;5(1):27. [PubMed: 18524244]

29. Connelly CM, Vogel WM, Wiegner AW, Osmers EL, Bing O, Kloner RA, et al. Effects of reperfusion after coronary artery occlusion on post-infarction scar tissue. Circulation research. 1985;57(4):562–77. [PubMed: 4042284]
30. Fomovsky GM, Macadangdang JR, Ailawadi G, Holmes JW. Model-based design of mechanical therapies for myocardial infarction. Journal of cardiovascular translational research. 2011;4(1):82–91. [PubMed: 21088945]
31. Gupta KB, Ratcliffe MB, Fallert MA, Edmunds L, Bogen DK. Changes in passive mechanical stiffness of myocardial tissue with aneurysm formation. Circulation. 1994;89(5):2315–26. [PubMed: 8181158]
32. Holmes JW, Covell JW. Collagen Fiber Orientation in Myocardial Scar Tissue Cardiovascular Pathobiology. 1996;1:15–22.
33. Weis SM, Emery JL, Becker KD, McBride DJ, Omens JH, McCulloch AD. Myocardial mechanics and collagen structure in the osteogenesis imperfecta murine (oim). Circulation research. 2000;87(8):663–9. [PubMed: 11029401]
34. Whittaker P, Boughner DR, Kloner R. Analysis of healing after myocardial infarction using polarized light microscopy. The American journal of pathology. 1989;134(4):879. [PubMed: 2705508]
35. Whittaker P, Kloner R, Boughner D, Pickering J. Quantitative assessment of myocardial collagen with picrosirius red staining and circularly polarized light. Basic research in cardiology. 1994;89(5):397–410. [PubMed: 7535519]
36. Reilly GC, Engler AJ. Intrinsic extracellular matrix properties regulate stem cell differentiation. Journal of biomechanics. 2010;43(1):55–62. [PubMed: 19800626]
37. Conrad C, Niess H, Huss R, Huber S, von Luettichau I, Nelson PJ, et al. Multipotent mesenchymal stem cells acquire a lymphendothelial phenotype and enhance lymphatic regeneration in vivo. Circulation. 2009;119(2):281–9. [PubMed: 19118255]
38. Friedland JC, Lee MH, Boettiger D. Mechanically activated integrin switch controls α5β1 function. Science. 2009;323(5914):642–4. [PubMed: 19179533]
39. Martino MM, Mochizuki M, Rothenfluh DA, Rempel SA, Hubbell JA, Barker TH. Controlling integrin specificity and stem cell differentiation in 2D and 3D environments through regulation of fibronectin domain stability. Biomaterials. 2009;30(6):1089–97. [PubMed: 19027948]
40. Rowlands AS, George PA, Cooper-White JJ. Directing osteogenic and myogenic differentiation of MSCs: interplay of stiffness and adhesive ligand presentation. American Journal of Physiology-Cell Physiology. 2008;295(4):C1037–C44. [PubMed: 18753317]
41. Yasunaga M, Tada S, Torikai-Nishikawa S, Nakano Y, Okada M, Jakt LM, et al. Induction and monitoring of definitive and visceral endoderm differentiation of mouse ES cells. Nature biotechnology. 2005;23(12):1542–50.
42. Ruiz SA, Chen CS. Emergence of patterned stem cell differentiation within multicellular structures. Stem cells. 2008;26(11):2921–7. [PubMed: 18703661]
43. Stevens MM, George JH. Exploring and engineering the cell surface interface. Science. 2005;310(5751):1135–8. [PubMed: 16293749]
44. Discher DE, Mooney DJ, Zandstra PW. Growth factors, matrices, and forces combine and control stem cells. Science. 2009;324(5935):1673–7. [PubMed: 19556500]
45. Berry MF, Engler AJ, Woo YJ, Pirolli TJ, Bish LT, Jayasankar V, et al. Mesenchymal stem cell injection after myocardial infarction improves myocardial compliance. American Journal of Physiology-Heart and Circulatory Physiology. 2006;290(6):H2196-H203.
46. Burdick JA, Vunjak-Novakovic G. Engineered microenvironments for controlled stem cell differentiation. Tissue Engineering Part A. 2008;15(2):205–19.
47. Winer JP, Janmey PA, McCormick ME, Funaki M. Bone marrow-derived human mesenchymal stem cells become quiescent on soft substrates but remain responsive to chemical or mechanical stimuli. Tissue Engineering Part A. 2008;15(1):147–54.
48. Huebsch N, Arany PR, Mao AS, Shvartsman D, Ali OA, Bencherif SA, et al. Harnessing tractionmediated manipulation of the cell/matrix interface to control stem-cell fate. Nature materials. 2010;9(6):518–26. [PubMed: 20418863]

49. Guan J, Wang F, Li Z, Chen J, Guo X, Liao J, et al. The stimulation of the cardiac differentiation of mesenchymal stem cells in tissue constructs that mimic myocardium structure and biomechanics. Biomaterials. 2011;32(24):5568–80. [PubMed: 21570113]
50. Li Z, Guo X, Palmer AF, Das H, Guan J. High-efficiency matrix modulus-induced cardiac differentiation of human mesenchymal stem cells inside a thermosensitive hydrogel. Acta biomaterialia. 2012;8(10):3586–95. [PubMed: 22729021]
51. Zaragoza C, Gomez-Guerrero C, Martin-Ventura JL, Blanco-Colio L, Lavin B, Mallavia B, et al. Animal models of cardiovascular diseases. BioMed Research International. 2011;2011.
52. Kraehenbuehl TP, Zammaretti P, Van der Vlies AJ, Schoenmakers RG, Lutolf MP, Jaconi ME, et al. Three-dimensional extracellular matrix-directed cardioprogenitor differentiation: systematic modulation of a synthetic cell-responsive PEG-hydrogel. Biomaterials. 2008;29(18):2757–66. [PubMed: 18396331]
53. Li Z, Guo X, Matsushita S, Guan J. Differentiation of cardiosphere-derived cells into a mature cardiac lineage using biodegradable poly (N-isopropylacrylamide) hydrogels. Biomaterials. 2011;32(12):3220–32. [PubMed: 21296413]
54. Xu Y, Patnaik S, Guo X, Li Z, Lo W, Butler R, et al. Cardiac differentiation of cardiosphere-derived cells in scaffolds mimicking morphology of the cardiac extracellular matrix. Acta biomaterialia. 2014;10(8):3449–62. [PubMed: 24769114]
55. Michaud K, Basso C, d'Amati G, Giordano C, Kholová I, Preston SD, et al. Diagnosis of myocardial infarction at autopsy: AECVP reappraisal in the light of the current clinical classification. Virchows Archiv 2020;476:179–94. [PubMed: 31522288]
56. Frangogiannis NG. Regulation of the inflammatory response in cardiac repair. Circulation research. 2012;110(1):159–73. [PubMed: 22223212]
57. Ma Y, Iyer RP, Jung M, Czubryt MP, Lindsey ML. Cardiac Fibroblast Activation Post-Myocardial Infarction: Current Knowledge Gaps. Trends Pharmacol Sci. 2017;38(5):448–58. [PubMed: 28365093]
58. Nielsen SH, Mouton AJ, DeLeon-Pennell KY, Genovese F, Karsdal M, Lindsey ML. Understanding cardiac extracellular matrix remodeling to develop biomarkers of myocardial infarction outcomes. Matrix Biol. 2017.
59. Lindsey ML, Mann DL, Entman ML, Spinale FG. Extracellular matrix remodeling following myocardial injury. Ann Med. 2003;35(5):316–26. [PubMed: 12952018]
60. DeLeon-Pennell KY, Meschiari CA, Jung M, Lindsey ML. Matrix Metalloproteinases in Myocardial Infarction and Heart Failure. Prog Mol Biol Transl Sci. 2017;147:75–100. [PubMed: 28413032]
61. Badylak SF, editor The extracellular matrix as a scaffold for tissue reconstruction. Seminars in cell & developmental biology; 2002: Elsevier.
62. Badylak SF. Xenogeneic extracellular matrix as a scaffold for tissue reconstruction. Transplant immunology. 2004;12(3–4):367–77. [PubMed: 15157928]
63. Gilbert TW, Sellaro TL, Badylak SF. Decellularization of tissues and organs. Biomaterials. 2006;27(19):3675–83. [PubMed: 16519932]
64. Badylak SF, Freytes DO, Gilbert TW. Extracellular matrix as a biological scaffold material: structure and function. Acta Biomaterialia. 2009;5(1):1–13. [PubMed: 18938117]
65. Badylak SF, Weiss DJ, Caplan A, Macchiarini P. Engineered whole organs and complex tissues. The Lancet. 2012;379(9819):943–52.
66. Crapo PM, Gilbert TW, Badylak SF. An overview of tissue and whole organ decellularization processes. Biomaterials. 2011;32(12):3233–43. [PubMed: 21296410]
67. Kim B-S, Baez CE, Atala A. Biomaterials for tissue engineering. World journal of urology. 2000;18(1):2–9. [PubMed: 10766037]
68. Liao J, Joyce EM, Sacks MS. Effects of decellularization on the mechanical and structural properties of the porcine aortic valve leaflet. Biomaterials. 2008;29(8):1065–74. [PubMed: 18096223]
69. Simon P, Kasimir M-T, Rieder E, Weigel G. Tissue Engineering of heart valves—Immunologic and inflammatory challenges of the allograft scaffold. Progress in Pediatric cardiology. 2006;21(2):161–5.

70. Fomovsky GM, Holmes JW. Evolution of scar structure, mechanics, and ventricular function after myocardial infarction in the rat. American Journal of Physiology-Heart and Circulatory Physiology. 2010;298(1):H221–H8. [PubMed: 19897714]
71. Gao E, Lei YH, Shang X, Huang ZM, Zuo L, Boucher M, et al. A novel and efficient model of coronary artery ligation and myocardial infarction in the mouse. Circulation research. 2010;107(12):1445–53. [PubMed: 20966393]
72. Sirry MS, Butler JR, Patnaik SS, Brazile B, Bertucci R, Claude A, et al. Characterisation of the mechanical properties of infarcted myocardium in the rat under biaxial tension and uniaxial compression. Journal of the mechanical behavior of biomedical materials. 2016;63:252–64. [PubMed: 27434651]
73. Wang B, Borazjani A, Tahai M, de Jongh Curry AL, Simionescu DT, Guan J, et al. Fabrication of cardiac patch with decellularized porcine myocardial scaffold and bone marrow mononuclear cells. Journal of Biomedical Materials Research Part A. 2010;94(4):1100–10. [PubMed: 20694977]
74. Wang B, Tedder ME, Perez CE, Wang G, de Jongh Curry AL, To F, et al. Structural and biomechanical characterizations of porcine myocardial extracellular matrix. Journal of Materials Science: Materials in Medicine. 2012;23(8):1835–47. [PubMed: 22584822]
75. Patnaik SS, Wang B, Weed B, Wertheim JA, Liao J. Chapter 3: Decellularized Scaffolds: Concepts, Methodologies, and Applications in Cardiac Tissue Engineering and Whole-Organ Regeneration. Tissue Regeneration: Where Nano-Structure Meets Biology: World Scientific; 2014. p. 77–124.
76. Grashow JS, Yoganathan AP, Sacks MS. Biaixal stress–stretch behavior of the mitral valve anterior leaflet at physiologic strain rates. Annals of biomedical engineering. 2006;34(2):315–25. [PubMed: 16450193]
77. Zhang S, Crow JA, Yang X, Chen J, Borazjani A, Mullins KB, et al. The correlation of 3D DT-MRI fiber disruption with structural and mechanical degeneration in porcine myocardium. Ann Biomed Eng. 2010;38(10):3084–95. [PubMed: 20499182]
78. Shi X, Liu Y, Copeland KM, McMahan SR, Zhang S, Butler JR, et al. Epicardial prestrained confinement and residual stresses: a newly observed heart ventricle confinement interface. J R Soc Interface. 2019;16(152):20190028.
79. Rezakhaniha R, Agianniotis A, Schrauwen JTC, Griffa A, Sage D, Bouten C, et al. Experimental investigation of collagen waviness and orientation in the arterial adventitia using confocal laser scanning microscopy. Biomechanics and modeling in mechanobiology. 2012;11(3–4):461–73. [PubMed: 21744269]
80. Junqueira LCU, Bignolas G, Brentani R. Picrosirius staining plus polarization microscopy, a specific method for collagen detection in tissue sections. The Histochemical journal. 1979;11(4):447–55. [PubMed: 91593]
81. Namba T, Tsutsui H, Tagawa H, Takahashi M, Saito K, Kozai T, et al. Regulation of fibrillar collagen gene expression and protein accumulation in volume-overloaded cardiac hypertrophy. Circulation. 1997;95(10):2448–54. [PubMed: 9170409]
82. Turner NA, Porter KE. Function and fate of myofibroblasts after myocardial infarction. Fibrogenesis Tissue Repair. 2013;6(1):5. [PubMed: 23448358]
83. Ertl G, Frantz S. Healing after myocardial infarction. Cardiovascular Research. 2005;66(1):22–32. [PubMed: 15769445]
84. Fomovsky GM, Rouillard AD, Holmes JW. Regional mechanics determine collagen fiber structure in healing myocardial infarcts. Journal of molecular and cellular cardiology. 2012;52(5):1083–90. [PubMed: 22418281]
85. Walkin L, Herrick SE, Summers A, Brenchley PE, Hoff CM, Korstanje R, et al. The role of mouse strain differences in the susceptibility to fibrosis: a systematic review. Fibrogenesis Tissue Repair. 2013;6(1):18. [PubMed: 24294831]
86. van den Borne SW, van De Schans VA, Strzelecka AE, Vervoort-Peters HT, Lijnen PM, Cleutjens JP, et al. Mouse strain determines the outcome of wound healing after myocardial infarction. Cardiovascular Research. 2009:cvp207.

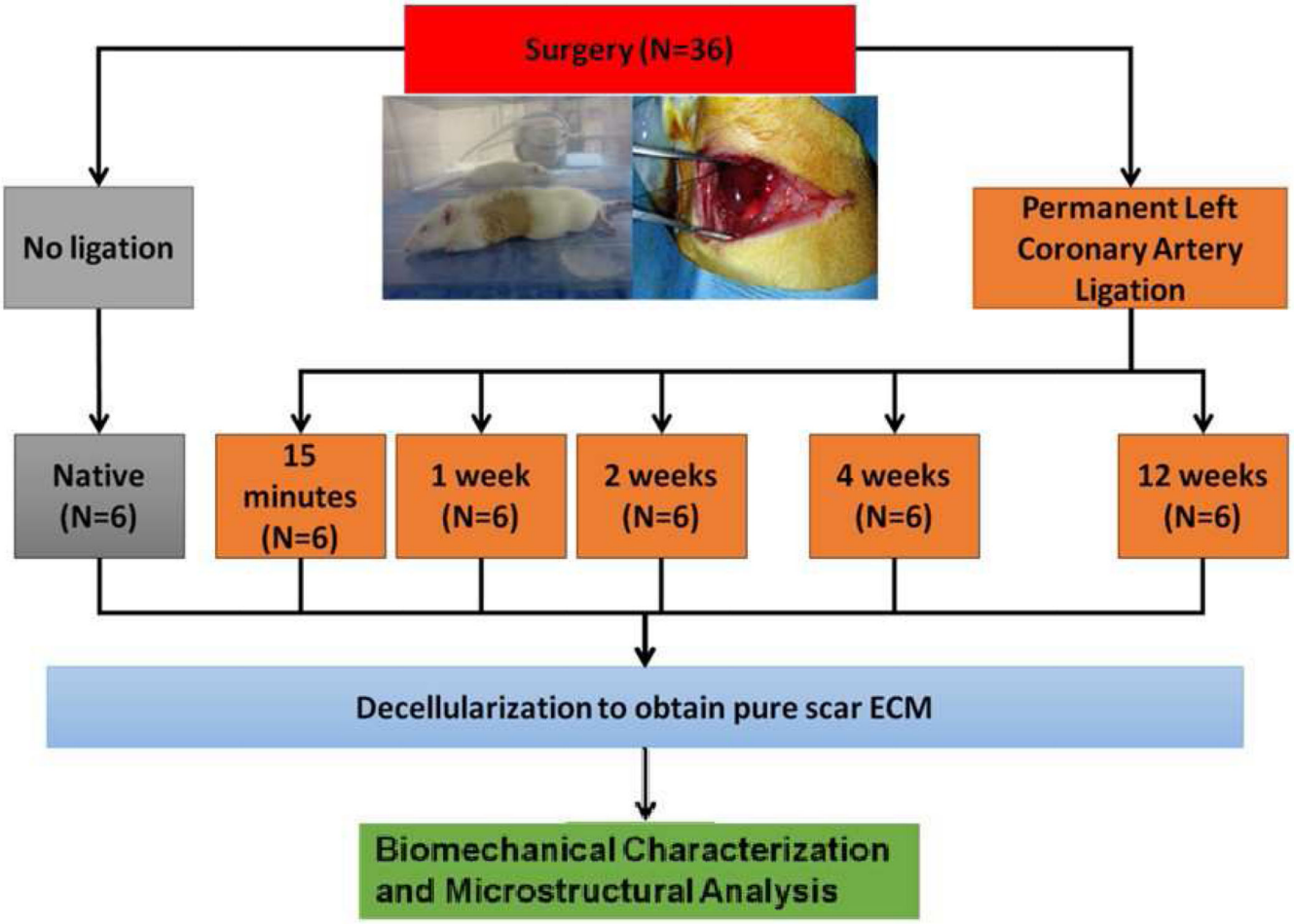

Figure 1:
Experimental design for the biomechanical study of the acellular scar ECM obtained from rat MI hearts via decellularization protocol and permanent left coronary artery ligation (PLCAL) model.

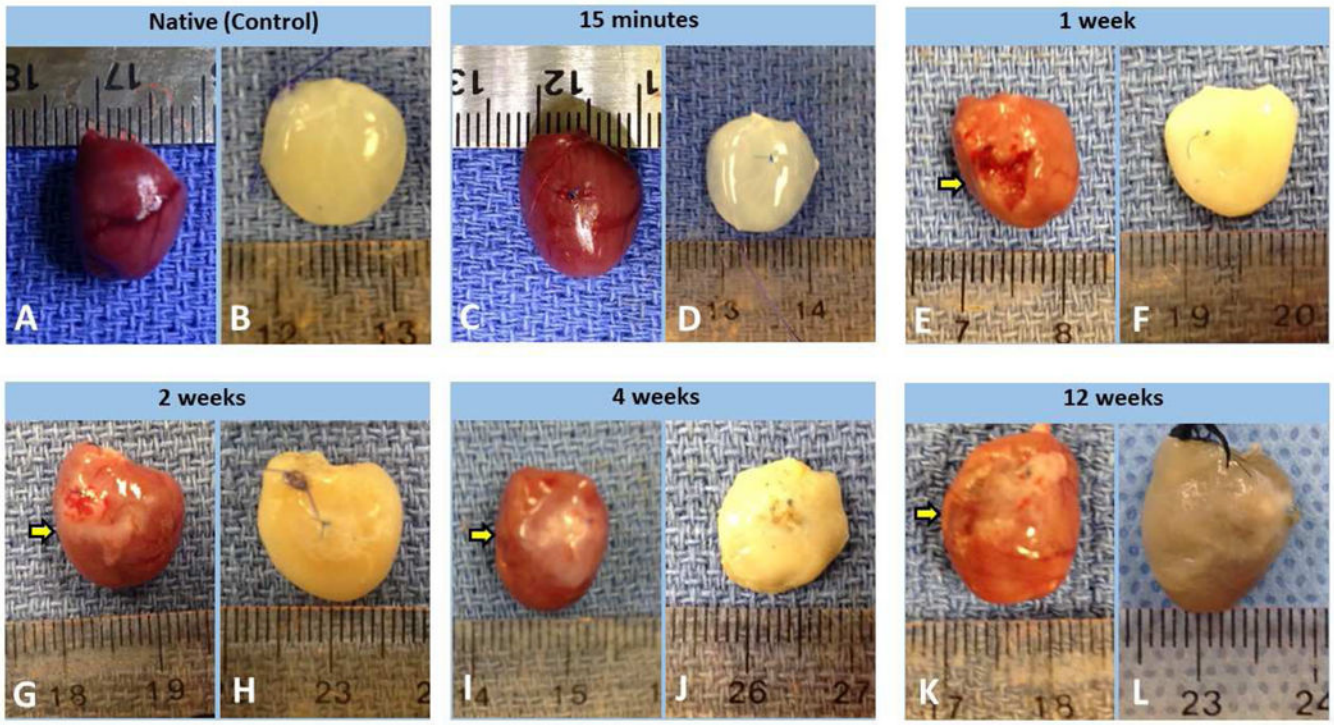

Figure 2:

Photos taken before decellularization and after decellularization of rat hearts from each time point post-MI. Native (control) group before (A) and after (B) decellularization; 15M post-MI group before (C) and after (D) decellularization; 1W scar group before (E) and after (F) decellularization; 2W scar group before (G) and after (H) decellularization; 4W scar group before (I) and after (J) decellularization; 12W scar group before (K) and after (L) decellularization. The MI-induced scar tissue with pale whitish color was labeled with Arrows in panel E, G, I, and K.

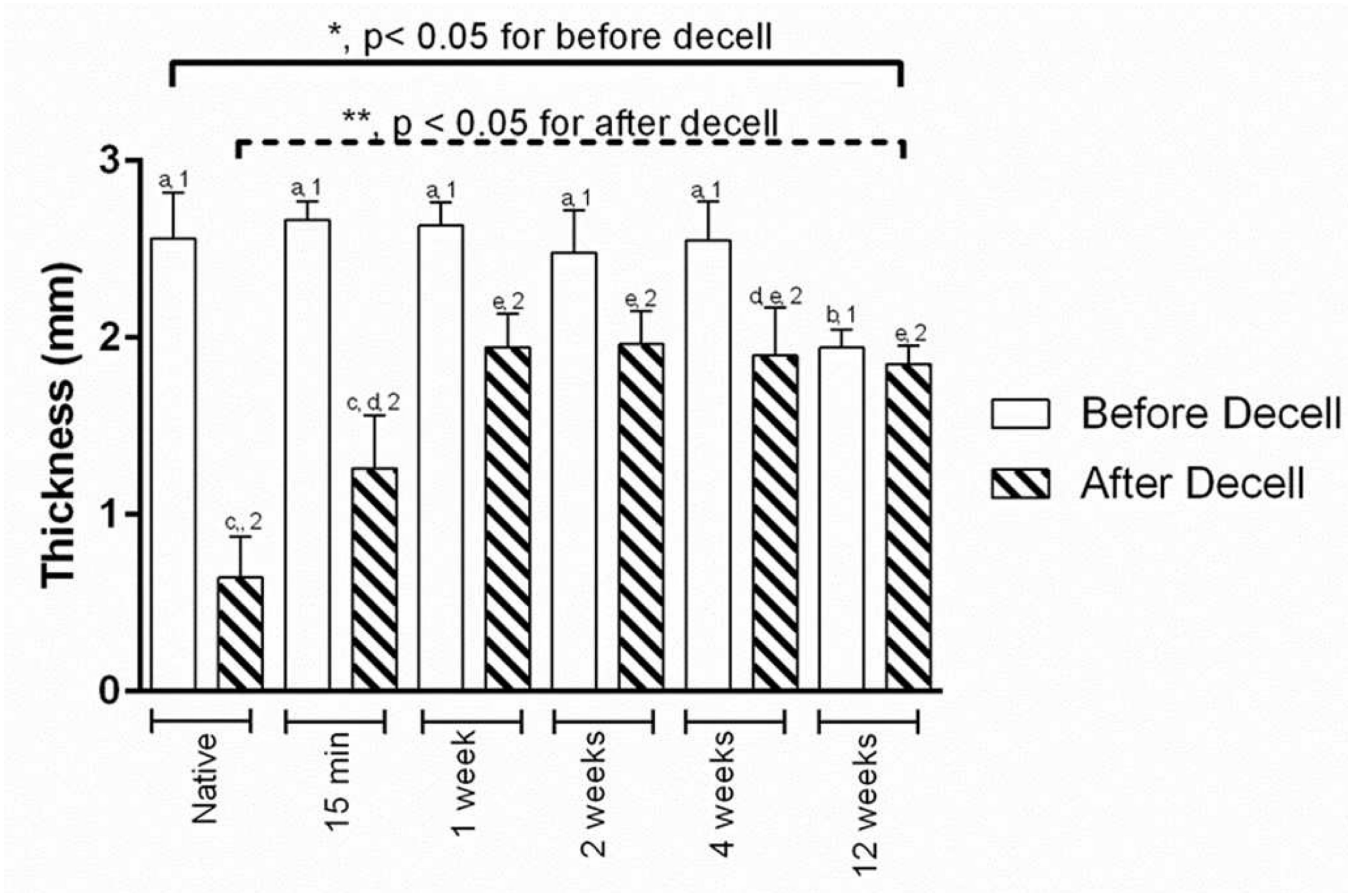

Figure 3:

Average wall thickness measurements from each group before and after decellularization treatment. Tukey's post hoc results for the before decellularization are shown with "a" or "b" to signify significant differences among the groups; whereas, Tukey's post hoc results for the after decellularization are shown with "c", "d", or "e" to signify significant differences among the groups. The paired t-test results are indicated with "1" or "2" to show a significant difference between the groups.

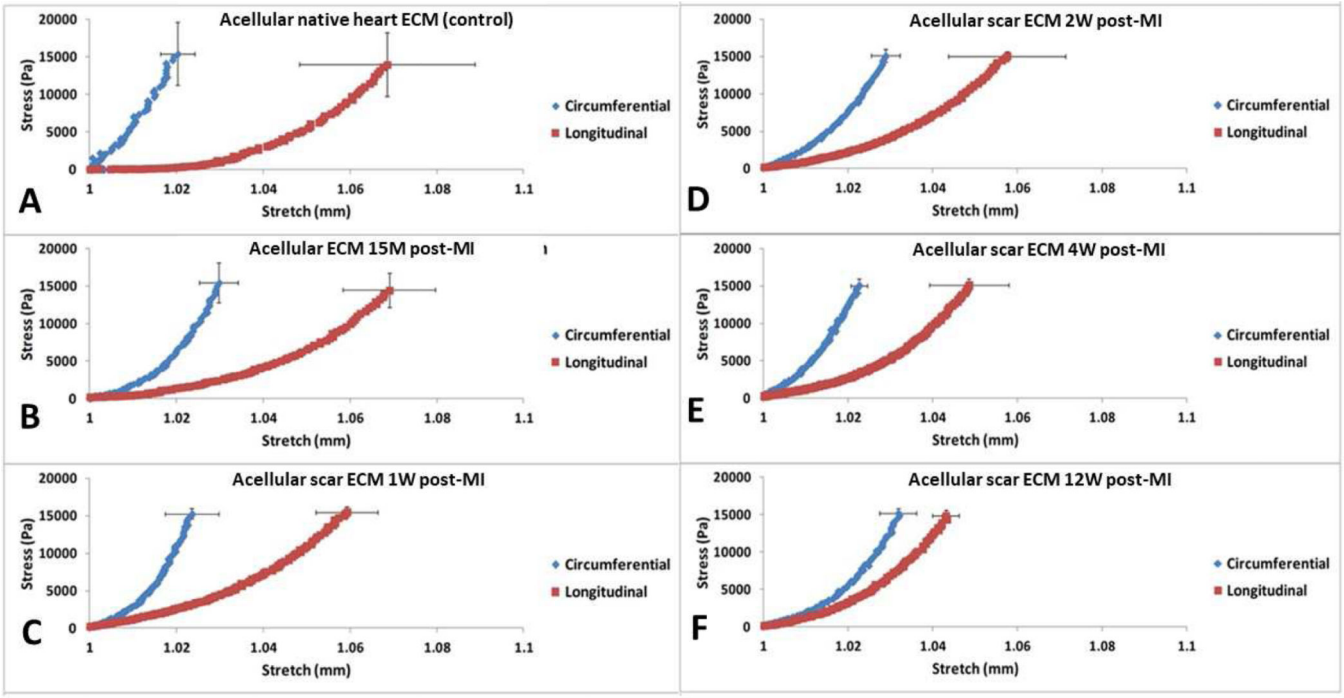

Figure 4:

Stress-stretch biaxial curves for (A) acellular native heart ECM (control group), (B) acellular ECM 15M post-MI, (C) acellular scar ECM 1W post-MI, (D) acellular scar ECM 2W post-MI, (E) acellular scar ECM 4W post-MI, and (F) acellular scar ECM 12W post-MI. The blue curve represents the circumferential direction; whereas the red curve represents the longitudinal direction. Error bars at the end of curves represent standard deviation.

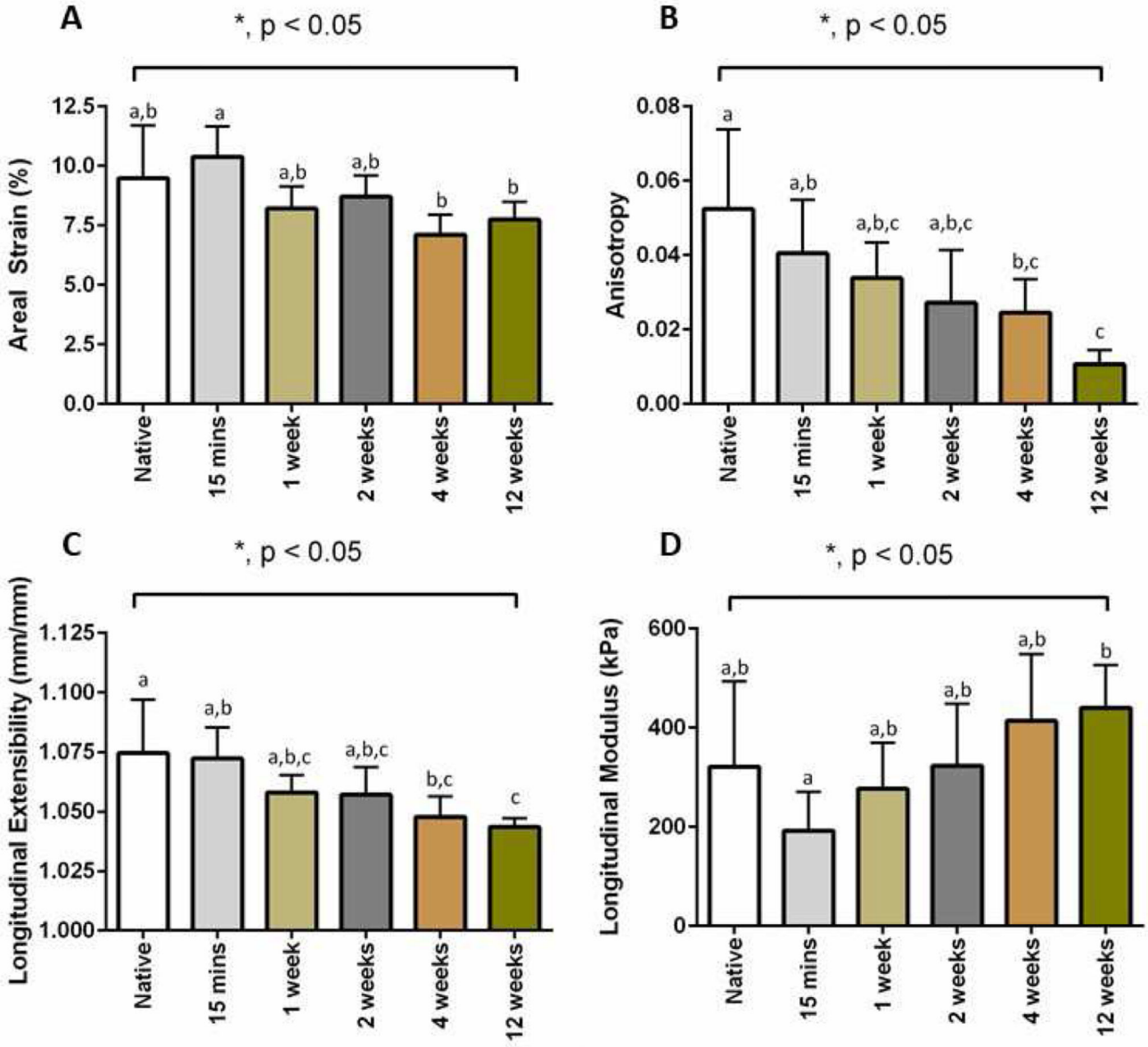

Figure 5:

Biaxial mechanical testing parameters results. (A) Areal strain for each time point. (B) Anisotropy index for each time point. (C) Longitudinal extensibility for each time point. (D) The longitudinal modulus for each time point. Tukey's post hoc results for each graph is indicated by the letters "a", "b", or "c" to signify significant differences among the groups.

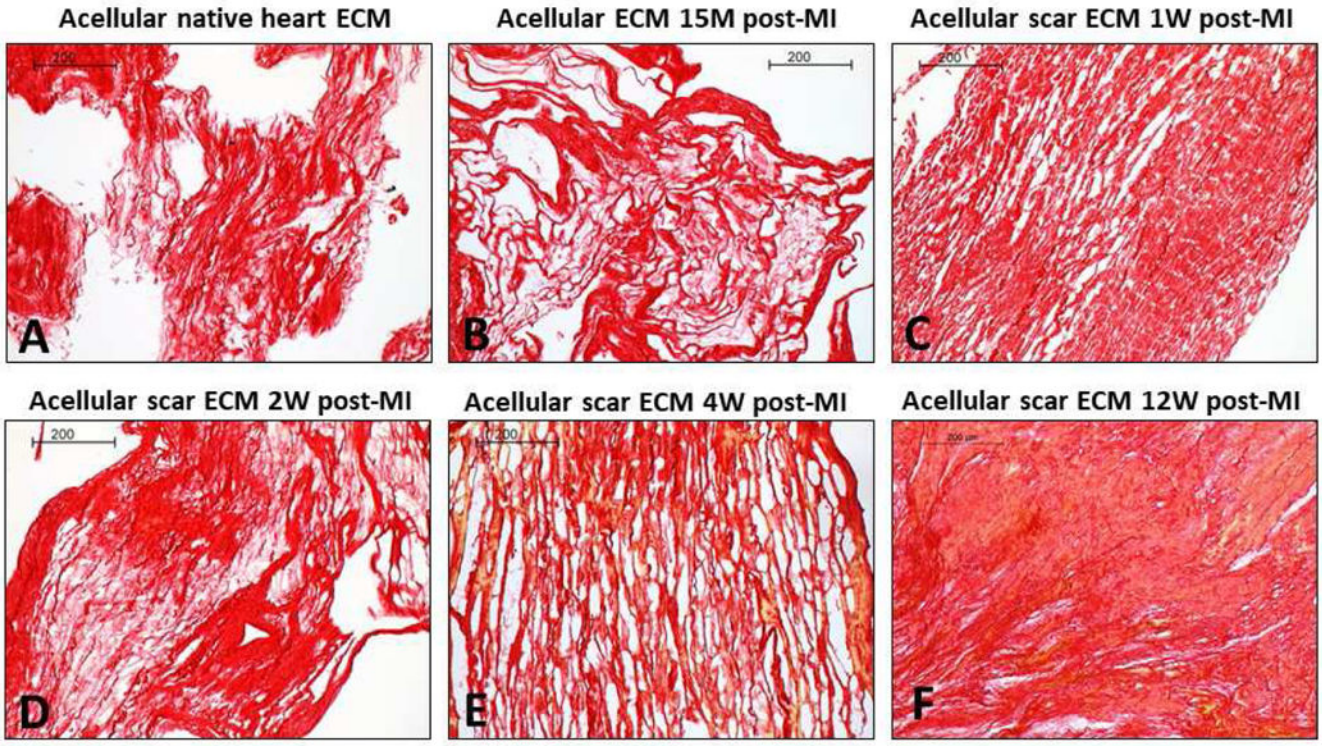

Figure 6:

Picrosirius red-stained histological images for (A) acellular native heart ECM (control group), (B) acellular ECM 15M post-MI, (C) acellular scar ECM 1W post-MI, (D) acellular scar ECM 2W post-MI, (E) acellular scar ECM 4W post-MI, and (F) acellular scar ECM 12W post-MI. Scale bars at 200 μm.

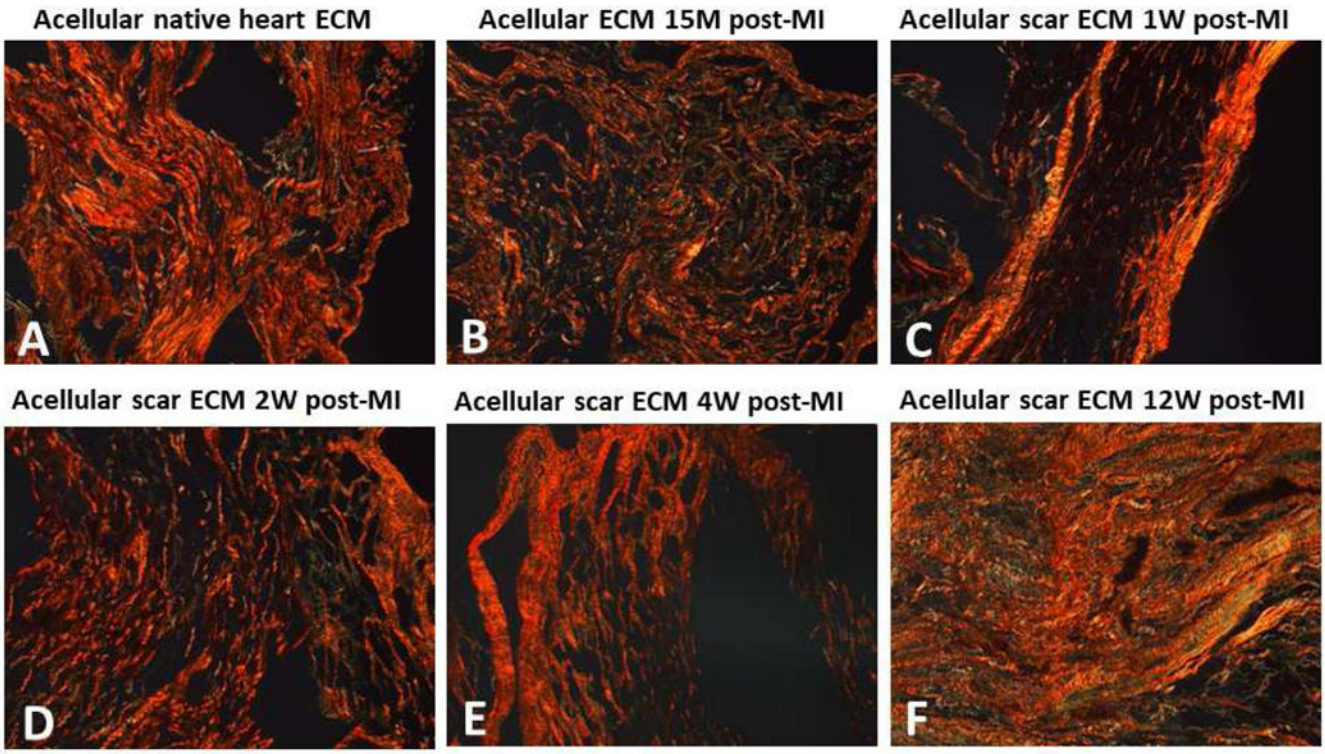

Figure 7:

Polarized light images from the picrosirius red-stained slides for (A) acellular native heart ECM (control group), (B) acellular ECM 15M post-MI, (C) acellular scar ECM 1W post-MI, (D) acellular scar ECM 2W post-MI, (E) acellular scar ECM 4W post-MI, and (F) acellular scar ECM 12W post-MI. Type I is yellow-red color and Type III collagen is green. Scale bars at 200 μm.

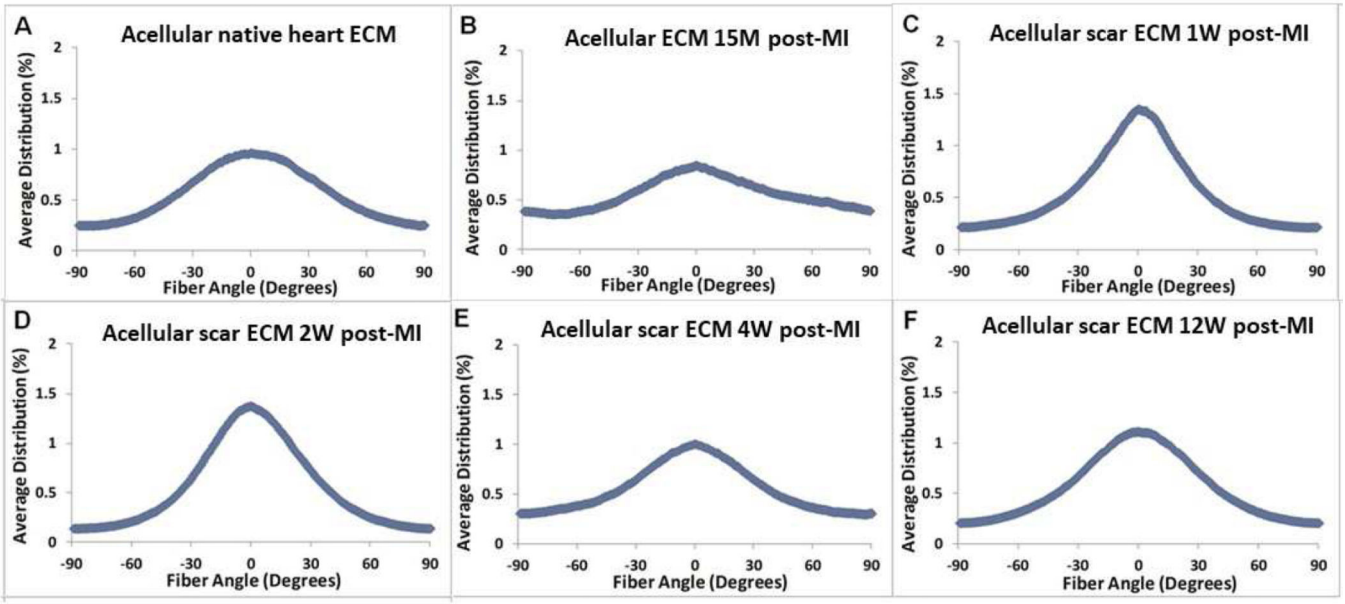

Figure 8:

Collagen fiber angular distribution quantified from picrosirius red-stained histological images for (A) acellular native heart ECM (control group), (B) acellular ECM 15M post-MI, (C) acellular scar ECM 1W post-MI, (D) acellular scar ECM 2W post-MI, (E) acellular scar ECM 4W post-MI, and (F) acellular scar ECM 12W post-MI.